



Deposited via The University of Sheffield.

White Rose Research Online URL for this paper:

<https://eprints.whiterose.ac.uk/id/eprint/208357/>

Version: Accepted Version

---

**Article:**

Yu, Y., Horoshenkov, K.V. and Tait, S. (2024) Microphone array analysis of the first non-axisymmetric mode for the detection of pipe conditions. *The Journal of the Acoustical Society of America*, 155 (1). pp. 575-587. ISSN: 0001-4966

<https://doi.org/10.1121/10.0024360>

---

© 2024 The Authors. Except as otherwise noted, this author-accepted version of a journal article published in *The Journal of the Acoustical Society of America* is made available via the University of Sheffield Research Publications and Copyright Policy under the terms of the Creative Commons Attribution 4.0 International License (CC-BY 4.0), which permits unrestricted use, distribution and reproduction in any medium, provided the original work is properly cited. To view a copy of this licence, visit <http://creativecommons.org/licenses/by/4.0/>

**Reuse**

This article is distributed under the terms of the Creative Commons Attribution (CC BY) licence. This licence allows you to distribute, remix, tweak, and build upon the work, even commercially, as long as you credit the authors for the original work. More information and the full terms of the licence here: <https://creativecommons.org/licenses/>

**Takedown**

If you consider content in White Rose Research Online to be in breach of UK law, please notify us by emailing [eprints@whiterose.ac.uk](mailto:eprints@whiterose.ac.uk) including the URL of the record and the reason for the withdrawal request.

# 1 **Microphone array analysis of the first non-axisymmetric mode for the detection of** 2 **pipe conditions**

3  
4 Yicheng Yu <sup>a,\*</sup>, Kirill V. Horoshenkov <sup>a</sup> and Simon Tait<sup>b</sup>

5 <sup>a</sup> Department of Mechanical Engineering, University of Sheffield, Mappin Street, Sheffield S1 3JD, UK.

6 <sup>b</sup> Department of Civil and Structural Engineering, University of Sheffield, Sheffield S1 3JD, UK

7 \* Corresponding author. E-mail address: Yicheng.Yu@sheffield.ac.uk

## 8 9 **Abstract**

10 This paper reports on the use of a circular microphone array to analyse the reflections from a pipe  
11 condition with enhanced resolution. A Bayesian maximum posteriori algorithm is combined with the  
12 mode decomposition approach to localize defects with six or less microphones. Unlike any previous  
13 acoustic reflectometry techniques that only estimate the location of a defect along the pipe, the proposed  
14 method uses the phase information about the wave propagated in the form of the first non-axisymmetric  
15 mode to estimate its circumferential position as well as axial location. The method is validated against  
16 data obtained from a laboratory measurement in a 150 mm diameter PVC pipe with a 20% in-pipe  
17 blockage and 100 mm lateral connection. The accuracy of localization of the lateral connection and  
18 blockage attained in this measurement was better than 2% of the axial sensing distance and 9° error in  
19 terms of the circumferential position. The practical significance of this approach is that it can be  
20 implemented remotely on an autonomous inspection robot so that accurate axial location and  
21 circumferential position of lateral connections and small blockages can be estimated with a  
22 computationally efficient algorithm.

## 1 **I. Introduction**

2 Underground infrastructure, particularly pipelines, plays a vital role in the transportation of various  
3 fluids, including water, oil, and gases, which are essential for urban life. In the United Kingdom, the  
4 length of sewer pipes and clean water pipes exceeds 600,000 km and 350,000 km, respectively [1],  
5 while in European Union countries, the length of drinking water and wastewater pipes is over 4.3  
6 million km and 3 million km, respectively [1]. The rapid aging and heavy usage of these pipelines due  
7 to population growth (larger volumes of wastewater), the rising demand for water, and the effects of  
8 climate change causing more intense rainfall events necessitate reliable techniques for monitoring the  
9 condition of pipes and detecting defects which may reduce the hydraulic carrying capacity of a pipe.

10 The advent of autonomous robotic sensing systems [2] within buried pipes has the potential to leverage  
11 recent progress with acoustic and ultrasonic sensing techniques for the purposes of condition monitoring  
12 and defects detection that can impact on hydraulic performance. In the past few decades, acoustic  
13 methods have been explored for assessing the condition and detecting blockages in sewage pipes [3].  
14 Compared to Closed-Circuit Television (CCTV), acoustic techniques require less power consumption  
15 and computation costs to make sense of data while having a significantly greater detection range.  
16 Acoustic echoes, including those reflected by blockages, can be remotely localized by measuring the  
17 time delay of the echoes with a microphone [4]. To expand the acoustic frequency range for detecting,  
18 localizing, and classifying blockages or lateral connections with a better accuracy, a circular  
19 microphone array was recently utilized on a robotic platform. This approach employed sparse  
20 representation and support vector machine methods [5]. Despite its efficacy, the aforementioned  
21 technique is limited in that it relies solely on plane wave measured by the averaging of the acoustic  
22 signal using a ring of microphones for axial localization of pipe conditions. Due to the uniform  
23 distribution of sound pressure in the plane wave across the pipe cross-section, this technique is unable  
24 to provide circumferential location information of pipe conditions, even though the analysed frequency  
25 range is above the cut-off frequencies. Higher modes (such as the first non-axisymmetric mode)  
26 overlooked in the previous studies, have circumferential sound pressure variation that can aid in  
27 identifying the circumferential location of pipe conditions. An array of microphones can be used to

1 select the desired higher-order modes. Advanced signal processing techniques, such as sparse  
2 representation [5] can now be leveraged to minimize the impact of mis-positioned or failed microphones  
3 to locate an artefact without any loss of accuracy.

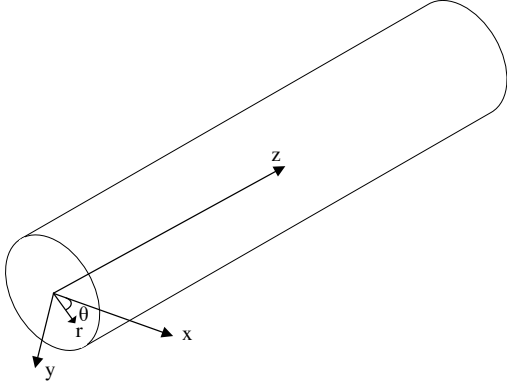
4 The present study makes use of a frequency domain algorithm based on Bayesian learning for the  
5 purpose of localizing pipe conditions axially and circumferentially. The proposed method employs an  
6 acoustic array and utilizes the first non-axisymmetric mode pattern via inverse estimation. Unlike the  
7 temporal approach described in reference [5], which applies direct deconvolution to estimate impulse  
8 response for robotic localization, the proposed frequency domain algorithm employs a Bayesian  
9 framework that accounts for the propagation term of the plane wave and the first mode (with frequency  
10 dependent propagation velocity) to estimate the location of pipe conditions straightforwardly.  
11 Furthermore, the proposed approach is shown to work even in the event when one of the six sensors  
12 becomes inoperable.

13 The structure of this paper is organised as follows. Section II discusses the theoretical framework of the  
14 Bayesian learning method to estimate the location of the defects in a pipe. The numerical simulation  
15 validation setup is discussed in Section III. Section IV presents the measurement setup of the pipe  
16 system and the data collected by a robotic platform with acoustic sensors. The estimation results using  
17 the Maximum a Posteriori method are presented and discussed in Section V.

18

## 1 II. Theory

### 2 A. Acoustic waves in a cylindrical pipe



3  
4 *Figure 1. The system of coordinates in a cylindrical pipe*

5 In the frequency domain the acoustic field in a rigid reflecting cylindrical pipe with the assumption of  
6 linearity (see Figure 1) can be expressed as the superposition of modes (e.g. [6]):

$$p(r, \theta, z, \omega) = \sum_{m,n} a_{mn} \varphi_{mn}(r, \theta) e^{-i\gamma_{mn}z} \quad (1)$$

7 where  $\omega$  is the angular frequency,  $m$  and  $n$  are the mode indices,  $\varphi_{mn}$  is the shape function for mode  
8  $(m, n)$ ,  $a_{mn}$  is the modal amplitude. For an air-filled cylindrical pipe with the radius  $R$  and acoustically  
9 rigid walls the mode shape function is given by [6]:

$$\varphi_{mn}(r, \theta) = \cos(m\theta) J_m(k_{mn}r) \quad (2)$$

10 where  $J_m(\cdot)$  denotes the  $m^{\text{th}}$  Bessel function. In a partially filled pipe, e.g. in a typical combined sewer  
11 pipe, the non-axisymmetric acoustic modes in Eq. (1) split and introduce extra complexity for the post-  
12 processing of acoustic data. The effect of water can be accounted for using the approach proposed in  
13 Ref. [7]. In this case the microphones are replaced with hydrophones or acoustic velocity sensors.

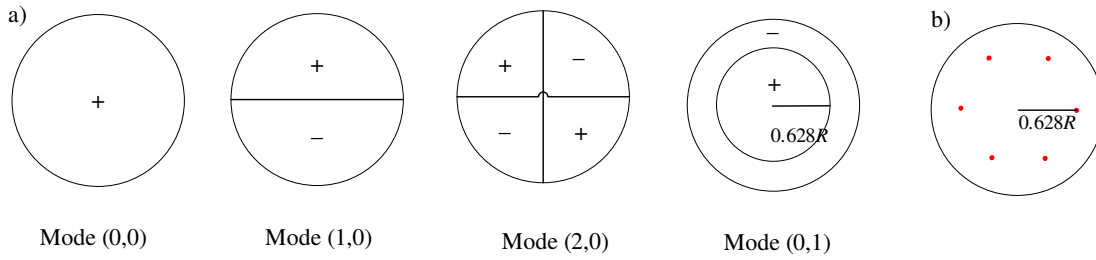
14 The eigen-number  $k_{mn}$  in Eq. (2) can be obtained from the zero normal velocity condition on the rigid  
15 wall of the pipe [6]:

$$J'_m(k_{mn}r)|_{r=R} = 0 \quad (3)$$

16 In the above equation  $'$  denotes partial derivative with respect to  $r$ . The  $z$ -axis wavenumber in Eq. (1)  
17 is then given by [6]:

$$\gamma_{mn} = \sqrt{k_0^2 - k_{mn}^2} \quad (4)$$

1 where  $k_0$  is the wavenumber in a free space ( $k_0 = \omega/c_0$ ,  $c_0$  is sound speed in air).  
 2 Eq. (4) predicts the wavenumber at which acoustic modes at different frequencies propagate along the  
 3 pipe. It is clear that  $\gamma_{mn}$  is frequency dependent, i.e., the acoustic propagation of these modes (except  
 4 in the case of plane wave when  $k_{00} = 0$ ) is dispersive. When the free field wavenumber  $k_0$  is larger  
 5 than the eigen-number  $k_{mn}$ , i.e. when the frequency of sound  $f > f_{mn}$ , where  $f_{mn} = k_{mn}c_0/(2\pi)$ , a  
 6 particular acoustic mode propagates along the pipe with relatively little attenuation at a velocity that is  
 7 dispersive. Figure 2(a) shows schematically the angular and radial dependence of the first four mode  
 8 shapes in the cylindrical pipe. In this figure the plus or minus correspond to the sign the modal shape,  
 9  $\varphi_{mn}$ , takes for a given values of  $\theta$  and  $r$  in Eq. (1).



10

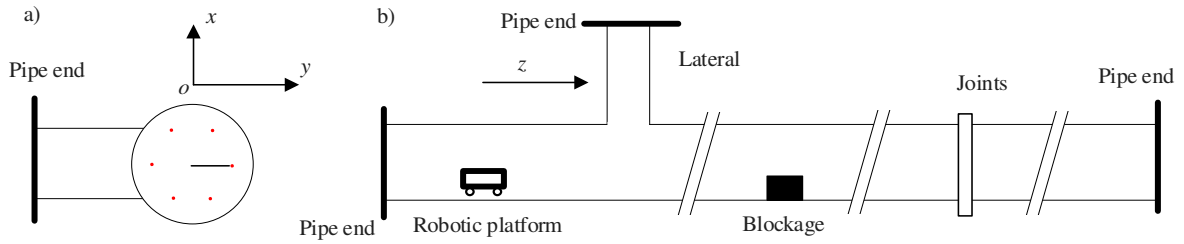
11 *Figure 2. An illustration of the behaviour of the first 4 modal shapes in the cylindrical pipe (a). The proposed arranged of the*  
 12 *six acoustic receivers to filter out individual modes (b).*

13 The work by Yu et al [5] used a six-microphone circular array to reconstruct the plane wave mode in  
 14 the frequency range well above the first cut-off frequency. The locations of the microphones in the array  
 15 are along the  $0.628 \cdot R$  circumference as shown in Figure 2(b). This enables the axisymmetric mode (0, 1)  
 16 to be filtered out and so cancel out the first two non-axisymmetric modes, (1, 0) and (2, 0), by averaging  
 17 the measured acoustic response and only extracting the plane wave, (0, 0) over a relatively broad  
 18 frequency range, e.g. up to 3 kHz in a 150 mm pipe. The plane wave mode was used in Ref. [5] to  
 19 localize blockages and lateral connections along the axial direction in the pipe, but it did not provide  
 20 any information on the circumferential position of these artefacts. This information is contained in the  
 21 first non-axisymmetric mode that was not analysed in the work reported in Ref. [5]. Furthermore, the

1 previous algorithm in Ref. [5] used sound pressure data from the six-microphone array to reconstruct  
 2 the plane wave mode. This requires all the microphones to be calibrated and to work in phase. If one of  
 3 the microphones in the array fails or is not calibrated (e.g. becomes contaminated with debris or wet),  
 4 it will be difficult to use the average of the rest of the microphone array data to reconstruct the plane  
 5 wave mode accurately.

6 This paper proposes a new algorithm to estimate the location of a pipe artefact or defect that does not  
 7 require a perfect functionality of all the microphones in the array shown in Figure 2(b). This algorithm  
 8 makes use of the plane wave, first non-axisymmetric mode and Bayesian learning to identify the axial  
 9 and circumferential positions of an artefact or defect in a pipe.

### 10 B. Axial and circumferential localization for pipe artefacts and defects



11  
 12 *Figure 3. (a) An array of six microphones in a circumferential array in a pipe with a lateral connection. (b) An illustration of*  
 13 *a pipe with a lateral connection, blockage, and joints and a robotic inspection platform with an acoustic array.*

14 In the frequency range  $f_{10} < f < f_{20}$  the first non-axisymmetric (1, 0) and plane wave modes (0, 0)  
 15 can propagate in a perfect pipe. If the acoustic source is located at the centre of the cross-section, only  
 16 a plane wave can be excited at these frequencies. If the pipe contains a non-axisymmetric artefact (e.g.  
 17 a lateral connection or blockage), a proportion of the incident wave is reflected and scattered in the form  
 18 of the plane wave first non-axisymmetric mode. These reflections can be detected with an array of  $Q$   
 19 microphones installed circumferentially as illustrated in Figure 2(b). The sound pressure at each of these  
 20 microphones is:

$$\begin{aligned}
 p_q(\theta_q, z, \omega) = & E(\omega)a_{00,q}e^{-2i\gamma_{00}z} \\
 & + E(\omega)a_{10,q} \cos(\theta_q - \theta_0) e^{-(i\gamma_{00}z + i\gamma_{10}z)} + n_q(\omega)
 \end{aligned}
 \tag{5}$$

21 where  $E(\omega)$  is the excitation signal which is usually a broad-band chirp (e.g. [5] [8]),  $q=1,2,3\dots Q$  is

1 the microphone index,  $n_q(\omega)$  is the noise recorded on the  $q^{\text{th}}$  microphone,  $\theta_q$  is the angular coordinate  
2 of the  $q^{\text{th}}$  microphone and  $\theta_0$  is the angular position of the artefact located at the distance from the array  
3  $z$ . The first term of the right side of Eq. (5) corresponds to the plane wave mode, and the second term  
4 is the first non-axisymmetric mode which contains the circumferential weighting  $\cos(\theta_q - \theta_0)$ . The  
5 phase term  $e^{-2i\gamma_{00}z}$  denotes the phase lag of the time of flight for the plane wave to propagate from the  
6 source and reflect from the artefact in the pipe. The second phase term in Eq. (5),  $e^{-(i\gamma_{00}z+i\gamma_{10}z)}$ ,  
7 denotes the phase lag for the plane wave as it travels from the source to the artefact with the wavenumber  
8  $\gamma_{00} = k_0$  to be reflected back as the first mode with the wavenumber  $\gamma_{10} = \sqrt{k_0^2 - \left(\frac{1.841}{R}\right)^2}$  (referred to  
9 Eq. (4) where  $k_{10} = \frac{1.841}{R}$ ). The reflected first non-axisymmetric mode carries information for the  
10 circumferential location of the artefact. To estimate the circumferential location of the artefact,  $\theta_0$  can  
11 be assumed as a variable  $\theta_v$  with totally  $V$  discretised angular patches. Eq. (5) can be rewritten as:

$$p_q(\theta_q, z, \omega) = E(\omega)a_{00,q}e^{-2i\gamma_{00}z} + \sum_{v=1}^V E(\omega)a_{10,v} \cos(\theta_q - \theta_v) e^{-(i\gamma_{00}z+i\gamma_{10}z)} + n_q(\omega) \quad (6)$$

12 In order to estimate the both the axial location and circumferential position of an artefact, Eq. (6) can  
13 be solved as an acoustic inverse problem against measured data. This problem can be written in the  
14 matrix form in the discrete frequency domain as:

$$\mathbf{p} = \mathbf{h}\mathbf{a} + \mathbf{n} \quad (7)$$

15 where  $\mathbf{p} = [p_1, p_2 \dots p_Q]^T$ ,  $\mathbf{h} = [h_{00}, h_{10,1}, h_{10,2} \dots h_{10,V}]$ ,  $\mathbf{a} = [a_{00}, a_{10,1}, a_{10,2} \dots a_{10,V}]^T$ .

16  $\mathbf{n} = [n_1, n_2 \dots n_Q]$  is the noise captured by the acoustic sensors.

17 The normalised (by the excitation) sound pressure spectrum estimated at  $L$  frequency points  $f_l$  is:

18  $p_q = [p_q(f_1)/E(f_1), \dots p_q(f_L)/E(f_L)]$ ,  $q = 1, 2 \dots Q$ .

19 The other quantities in Eq. (7) are:

$$1 \quad \mathbf{h}_{00} = \begin{bmatrix} \mathbf{h}_{00,1} \\ \mathbf{h}_{00,2} \\ \dots \\ \mathbf{h}_{00,Q} \end{bmatrix}; \mathbf{h}_{00,q} = \begin{bmatrix} e^{-2i\gamma_{00}(f_1)z_1} & e^{-2i\gamma_{00}(f_1)z_2} & \dots & e^{-2i\gamma_{00}(f_1)z_J} \\ e^{-2i\gamma_{00}(f_2)z_1} & e^{-2i\gamma_{00}(f_2)z_2} & \dots & e^{-2i\gamma_{00}(f_2)z_J} \\ \vdots & \vdots & \ddots & \vdots \\ e^{-2i\gamma_{00}(f_L)z_1} & e^{-2i\gamma_{00}(f_L)z_2} & \dots & e^{-2i\gamma_{00}(f_L)z_J} \end{bmatrix};$$

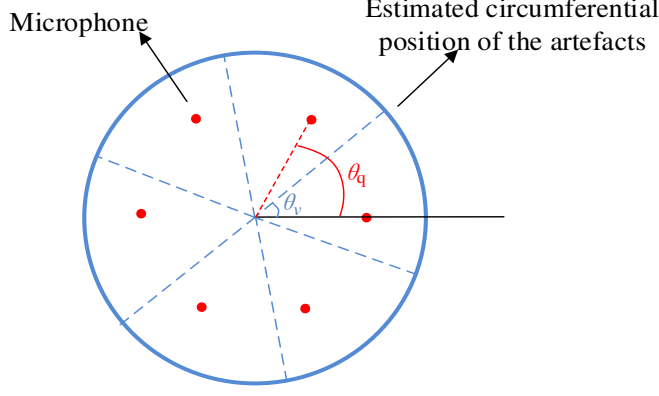
$$2 \quad \mathbf{h}_{10,v} = \begin{bmatrix} \mathbf{h}_{10,1v} \\ \mathbf{h}_{10,2v} \\ \dots \\ \mathbf{h}_{10,Qv} \end{bmatrix}, v = 1, 2 \dots V$$

$$3 \quad \mathbf{h}_{10,qv} = \cos(\theta_q - \theta_v) \begin{bmatrix} e^{-i[\gamma_{10}(f_1)+\gamma_{00}(f_1)]z_1} & e^{-i[\gamma_{10}(f_1)+\gamma_{00}(f_1)]z_2} & \dots & e^{-i[\gamma_{10}(f_1)+\gamma_{00}(f_1)]z_J} \\ e^{-i[\gamma_{10}(f_2)+\gamma_{00}(f_2)]z_1} & e^{-i[\gamma_{10}(f_2)+\gamma_{00}(f_2)]z_2} & \dots & e^{-i[\gamma_{10}(f_2)+\gamma_{00}(f_2)]z_J} \\ \vdots & \vdots & \ddots & \vdots \\ e^{-i[\gamma_{10}(f_L)+\gamma_{00}(f_L)]z_1} & e^{-i[\gamma_{10}(f_L)+\gamma_{00}(f_L)]z_2} & \dots & e^{-i[\gamma_{10}(f_L)+\gamma_{00}(f_L)]z_J} \end{bmatrix}$$

$$4 \quad \mathbf{a}_{00} = [a_{00}(z_1), a_{00}(z_2) \dots a_{00}(z_J)]; \mathbf{a}_{10,v} = [a_{10,v}(z_1), a_{10,v}(z_2) \dots a_{10,v}(z_J)].$$

5 In the above equations  $z_j$  is the spatial coordinate of the pipe,  $L$  and  $J$  are the total numbers of the  
6 frequency and distance points, respectively. In the following text we occasionally refer to the amplitudes  
7  $a_{00}(z_j)$  and  $a_{10,v}(z_j)$  in Eq. (7) as  $a_j$ . In order to estimate the circumferential position of the artefact,  
8 the cross-section is discretized into  $V$  sections.  $Q$  and  $V$  are the total numbers of the microphones in the  
9 array and the estimated circumferential artefacts points, respectively. The circumferential coordinate of  
10 the  $q^{\text{th}}$  microphone is at  $\theta_q$ , and the estimated artefacts at  $\theta_v$ . When the estimated artefact is located at  
11  $\theta_{v'}$ , then the corresponding amplitude term  $\mathbf{a}_{10,v'}$  is expected to have a relatively significant value,  
12 otherwise the amplitude term  $\mathbf{a}_{10,v'}$  should be zero.

13 In this paper  $V$  is assumed equal to the total number of the microphones, which means  $V=Q$ . When  $LQ$   
14 is larger than  $JV$  (or  $L>J$  since  $V=Q$ ), the inverse problem of Eq. (7) is over-determined and can be  
15 solved using the Least Square (LS) method, for example the LSQR algorithm [9]. Therefore, the number  
16 of microphones in the array can affect the circumferential resolution for the detection of  
17 artefacts/defects in the pipe. On the other hand, if  $LQ$  is smaller than  $JV$ , the inverse problem of Eq. (7)  
18 is under-determined. This paper proposes a sparse representation method to solve it, which is also  
19 known as compressive sensing [10].



1

2 *Figure 4. illustration of the circumferential position of microphones and the estimated artefacts.*

### 3 **C. Bayesian learning**

4 In this paper, Bayesian learning is used for the linear inverse problem in Eq (7). Bayesian learning is a  
 5 method to estimate a random process from a related observation signal and prior knowledge of the  
 6 probability distribution of this process. There are many classical estimators used in Bayesian philosophy  
 7 such as: maximum a posteriori (MAP), and minimum mean relative value of error (MAVE) [11]. This  
 8 paper uses the MAP method for the estimation of pipe conditions.

9 The probability density function (pdf)  $\mathcal{P}$  of the artefact's amplitude vector  $\mathbf{a}$  given an observation for  
 10 the acoustic response  $\mathbf{p}$  can be described as [11]:

$$\mathcal{P}(\mathbf{a}|\mathbf{p}) = \frac{\mathcal{P}(\mathbf{p}|\mathbf{a})\mathcal{P}(\mathbf{a})}{\mathcal{P}(\mathbf{p})} \quad (8)$$

11 The likelihood of the signal  $\mathbf{p}$  given the artefacts amplitude vector  $\mathbf{a}$  can be assigned a Gaussian  
 12 distribution that is a rigorous result of the maximum entropy principle [12]. This function describes the  
 13 distribution of the residue errors between the measured sound pressure and the prediction model,  
 14  $(\mathbf{p} - \mathbf{h}\mathbf{a})$  [12], i.e.

$$\mathcal{P}(\mathbf{p}|\mathbf{a}) = \frac{1}{(2\pi\sigma_n^2)^{\frac{L}{2}}} \exp \left[ -\frac{1}{2\sigma_n^2} (\mathbf{p} - \mathbf{h}\mathbf{a} - \boldsymbol{\mu})^H (\mathbf{p} - \mathbf{h}\mathbf{a} - \boldsymbol{\mu}) \right] \quad (9)$$

15 where  $H$  is the conjugate transpose,  $\boldsymbol{\mu}$  and  $\sigma$  are the mean and constant covariance of the residue error,  
 16 respectively. The MAP estimate  $\hat{\mathbf{a}}_{MAP}$  is obtained as the artefacts amplitude vector that maximises the  
 17 posterior pdf:

$$\hat{\mathbf{a}}_{MAP} = \arg \max_{\mathbf{a}} \mathcal{P}(\mathbf{a}|\mathbf{p}) = \arg \max_{\mathbf{a}} \frac{\mathcal{P}(\mathbf{p}|\mathbf{a})\mathcal{P}(\mathbf{a})}{\mathcal{P}(\mathbf{p})} \quad (10)$$

1 In general, in order to avoid any subjective injection into the process, uniform distribution of  $\mathbf{a}$  can be  
 2 assigned due to the non-informative prior using the principle of maximum entropy [12, 13]. This paper  
 3 makes use of the sparsity of any defect/artefact's amplitude  $\mathbf{a}$  in Eq. (7). The sparse nature of defects  
 4 and artefacts (e.g. blockages or joints) is common in drainage pipes. It has been illustrated in Ref. [8,  
 5 5] that the sparsity of impulse response in the pipe can be observed in the time domain and wavelet  
 6 domain. The sparse nature of in-pipe defects and artefacts suggests the use of a Laplacian distribution  
 7 [15, 16]. In this case, the defect/artefact's amplitude  $\mathbf{a}$  with sparsity is modelled empirically with the  
 8 probability that has a sharp maximum and long tail distribution.

9 The assignment of the Laplacian prior can be understood as a two-stage hierarchical model. At the first  
 10 stage of a hierarchical model, a normality (Gaussian) prior is employed [15, 16]:

$$\mathcal{P}(\mathbf{a}|\boldsymbol{\beta}) = \prod_{j=1}^J \mathcal{N}(a_j|0, \beta_j) \quad (11)$$

11 where  $\beta_j$  is amplitude variance and  $\mathcal{N}(a_j|0, \beta_j)$  is the Gaussian function.  $\boldsymbol{\beta}$  is also called  
 12 *hyperparameter* of the model and the additional prior distribution is called *hyperprior*. At the second  
 13 stage, each  $\beta_j$  is modelled as an exponentially decaying Laplacian (hyper)prior [15, 16]:

$$\mathcal{P}(\beta_j|\zeta) = \frac{\zeta}{2} \exp\left(-\frac{\zeta}{2}\beta_j\right) \quad (12)$$

14 where  $\zeta$  is the parameter of the exponential prior that is adjusted by the regularization algorithm. Then  
 15 it is possible to integrate out  $\beta_j$  by [15, 16]:

$$\begin{aligned} \mathcal{P}(\mathbf{a}|\zeta) &= \int \mathcal{P}(\mathbf{a}|\boldsymbol{\beta})\mathcal{P}(\boldsymbol{\beta}|\zeta) d\boldsymbol{\beta} = \prod_{j=1}^J \int \mathcal{P}(a_j|\beta_j)\mathcal{P}(\beta_j|\zeta) d\beta_j \\ &= \frac{\zeta^{\frac{J}{2}}}{2^J} \exp\left(-\zeta^{\frac{1}{2}} \sum_{j=1}^J |a_j|\right) \end{aligned} \quad (13)$$

16 Therefore, the prior is assigned to Laplacian to account for the sparsity [15, 16]:

$$\mathcal{P}(\mathbf{a}) \propto \exp\left[-\zeta^{\frac{1}{2}}\|\mathbf{a}\|_1\right] \quad (14)$$

1 In this case, the posterior distribution can be obtained by substituting Eqs. (9),(14) into Eq. (10):

$$\mathcal{P}(\mathbf{a}|\mathbf{p}) = \frac{1}{\mathcal{P}(\mathbf{p})} \frac{1}{(2\pi\sigma_n)^{\frac{L}{2}}} \frac{1}{(2\pi)^{\frac{L}{2}}|\zeta|^{-\frac{L}{2}}} \exp\left[-\frac{1}{2\sigma_n^2}(\mathbf{p} - \mathbf{h}\mathbf{a} - \boldsymbol{\mu})^H(\mathbf{p} - \mathbf{h}\mathbf{a} - \boldsymbol{\mu}) - \zeta^{\frac{1}{2}}\|\mathbf{a}\|_1\right] \quad (15)$$

2 The MAP estimation of the artefacts can then be obtained by differentiating the log-posterior pdf,

3  $\ln[\mathcal{P}(\mathbf{a}|\mathbf{p})]$ , and setting the derivative to zero so that the MAP estimate is [14]:

4

$$\hat{\mathbf{a}} = \arg \min_{\mathbf{a}} \left\{ \frac{1}{2}\|\mathbf{p} - \mathbf{h}\mathbf{a} - \boldsymbol{\mu}\|_2^2 + \lambda\|\mathbf{a}\|_1 \right\} \quad (16)$$

5 where  $\lambda$  is known as the regularization parameter  $\lambda = \zeta^{\frac{1}{2}}\sigma_n^2$  and the hat sign denotes the estimate.

6 This is also called the  $\ell_1$ -norm regularization, which describes the sum of absolute values of the

7 elements of  $\hat{\mathbf{a}}$ . The  $\ell_1$ -norm is commonly used to induce sparsity in the optimal solution of Eq. (16). In

8 this paper the  $\ell_1$ -norm regularization is solved using the SpaRSA algorithm [17]. After estimating the

9 amplitude vector  $\hat{\mathbf{a}}$ , the location of the artefacts can be obtained directly from the non-zero components

10  $a_j$  associated to its axial coordinates  $z_j$ . The proposed technique for the localization of artefacts in the

11 pipe with mobile compensation using  $\ell_1$ -norm regularization is summarized in Table 1.

12 *Table 1. The algorithm for frequency domain with  $\ell_1$ -norm regularization using SpaRSA [17] to localize artefacts/defects in*

13 *a pipe.*

Task: To estimate the location of defects/artefacts in the pipe $\hat{\mathbf{a}}$
Input: Excitation chirp signal $E(t)$ , response signal from the six microphones in the array, $\mathbf{p}_m(t)$ $m=1:6$
Fast Fourier transform: $\mathbf{p}(\omega) = \mathcal{FFT}\{\mathbf{p}(t)\}$ , $E(\omega) = \mathcal{FFT}\{E(t)\}$ ,
Transfer matrix: $\mathbf{h}(\omega, \mathbf{z}_j)$ with elements listed in Eq. (7)

Initialization: Set the iteration number to  $k=1$ ,  $\mathbf{A} = \mathbf{h}$ ,  $\mathbf{x}_1 = \mathbf{p}$ ,  $\tau_1 \mathbf{I} = \mathbf{A}^T \mathbf{A}$ , tolerance  $\varepsilon = 10^{-5}$  [17], parameter  $\lambda = 0.001$  [17]

Iteration:

1.  $\lambda_k = \max\{0.1\|\mathbf{A}^T \mathbf{x}_k\|_\infty, \lambda\}$  [17].

2. Exploit soft shrinkage [17]:  $\mathbf{a}_{k+1} = \text{shrink}(\mathbf{a}_k - \mathbf{A}^T(\mathbf{A}\mathbf{a}_k - \mathbf{x})/\tau_k, \lambda_k/\tau_k)$

(where  $\text{shrink}(a_k, \lambda) = \text{sign}(a_k) \max\{|a_k| - \lambda, 0\}$ )

3. Update the step size [17]:  $\tau_k = \frac{(\mathbf{a}_{k+1} - \mathbf{a}_k)^T (\nabla \vartheta(\mathbf{a}_{k+1}) - \nabla \vartheta(\mathbf{a}_k))}{(\mathbf{a}_{k+1} - \mathbf{a}_k)^T (\mathbf{a}_{k+1} - \mathbf{a}_k)}$

4. If  $\frac{\|\mathbf{a}_{k+1} - \mathbf{a}_k\|}{a_k} \leq \varepsilon$ , go to step 5. Otherwise, return to step 2 [17]

5.  $\mathbf{a}_{k+1} = \mathbf{x} - \mathbf{A}\mathbf{a}_{k+1}$

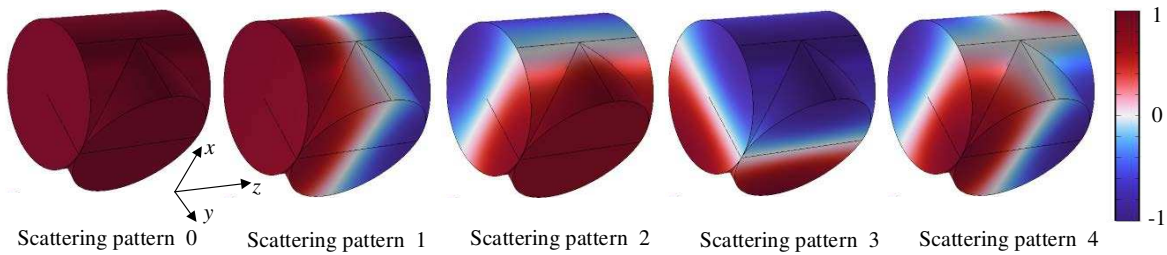
6. If  $\lambda_k \leq \lambda$ , stop; Otherwise  $k=k+1$ , and return to step 1.

Output:  $\hat{\mathbf{a}} = \mathbf{a}_k$

1

### 2 III. Simulations

3 An acoustic wave propagates in a pipe and scatters due to the existence of any artefacts/defects, e.g.  
 4 lateral connections or blockages. Figure 5 presents the five possible scattered wave patterns from a  
 5 lateral connection. This simulation was using the eigen-frequency analysis of a Finite Element Analyzer  
 6 (FEA) such as COMSOL, where the plane wave and first non-axisymmetric modes in the main pipe  
 7 and lateral connection were analysed. The FEA uses the mesh size around 0.01 m which is less than  
 8 1/10 of the wavelength of the highest frequency at 3 kHz. The diameter of the main pipe and the side  
 9 branch is 150 mm diameter.

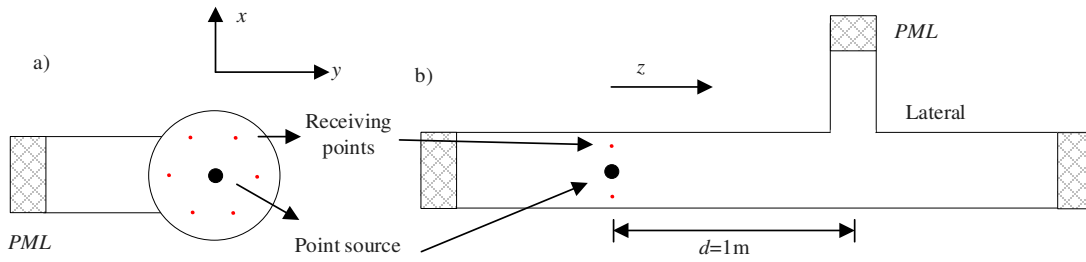


11 *Figure 5. An illustration of scattering wave patterns at a lateral connection, z-axis is the axial direction of the main pipe.*

1 Assuming that the analysed frequency range is  $f_{10} < f < f_{20}$ , only plane wave travels along the pipe with a  
2 point source excitation located at the centre of the pipe. This happens because the source is located at  
3 the nodal position of the first non-axisymmetric mode, whereas the first axisymmetric mode (0, 1) is  
4 evanescent and does not propagate. Therefore, the scattered/reflected wave from the lateral connection  
5 is due to the incident plane wave. The scattered wave contains the plane wave mode and the first wave  
6 mode. As illustrated in Figure 5, the plane wave pattern denoted as Pattern 0 characterizes a uniform  
7 sound pressure amplitude across both the main pipe and lateral branch during its propagation. Pattern 1  
8 signifies the occurrence of a plane wave in the main pipe coupled with the first non-axisymmetric mode  
9 in the branch. Similarly, Pattern 2 represents the manifestation of the first mode in the main pipe along  
10 with a plane wave in the branch. Patterns 3 and 4 depict scenarios where the first mode is present in the  
11 main pipe, coexisting with the lateral connection branch.

12 As discussed previously, in this frequency range only plane wave can be excited along the main pipe  
13 with a point source excitation at the centre of the pipe cross-section. With the symmetry of the plane  
14 wave incidence and the symmetry of the boundary condition of the lateral connection with respect to  
15 the plane  $x=0$  (see Figure 5), the scattered wave from lateral connection is expected to be symmetric  
16 with respect to the plane  $x=0$  (see Figure 5). For example, Pattern 3, which is anti-symmetric with  
17 respect to the plane  $x=0$ , should be cancelled. Therefore, only patterns 0, 1, 2 and 4 (see Figure 5) can  
18 be excited. As shown in patterns 2, and 4, the maximum amplitude of the first mode corresponds to the  
19 location of the lateral connection. This physics can be used to estimate the circumferential position of  
20 the lateral pipe by analysing the amplitude and phase in the sound pressure recorded on the microphone  
21 array. This will be validated with simulation and measurements in the following discussion.

22 In order to ensure that Eq. (7) is not under-determined, the number of estimated points  $V$  should be no  
23 less than the number of microphone array  $Q$ , where it is assumed that  $V=Q$  in this study. This means  
24 that the possible location of defects/artefacts is discretized into  $V$  sectors circumferentially. Therefore,  
25 the number of the microphone array sensor can affect the circumferential resolution of the proposed  
26 defect/artefact localization method.



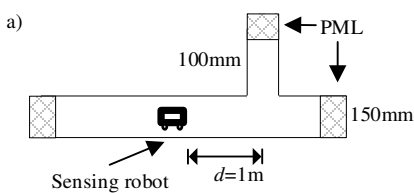
1

2 *Figure 6. An illustration of the sensing system arrangement in a pipe with a lateral connection used in the FEA simulation.*

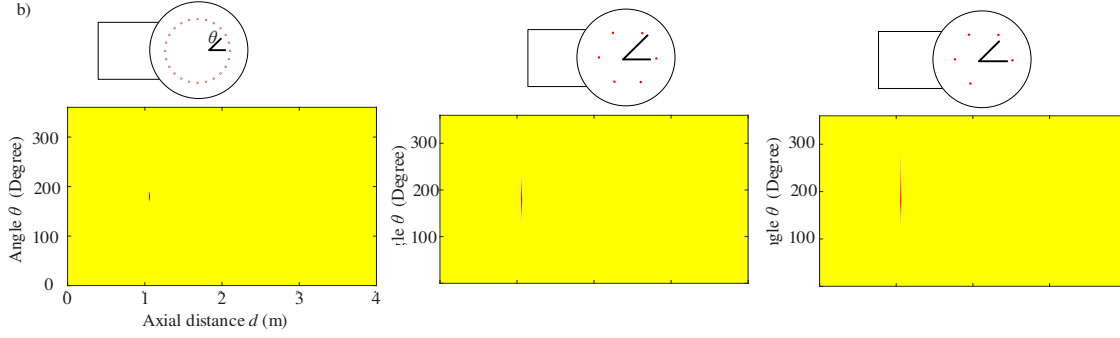
3 *Side view (a). Top view (b).*

4 This numerical simulation using frequency domain FEA (see Figure 6) was carried out to study the  
 5 effect of the number of microphones on the quality of the defect localization. The frequency range in  
 6 this numerical study was 1500-2000 Hz, with 1 Hz resolution. Perfect Matched Layer (PML) [18] was  
 7 set up at the ends of the pipe to simulate an infinite pipe length. The excitation amplitude was uniform  
 8 over the frequency range. Using the Bayesian theory with SpaRSA algorithm, Eq. (7) can be solved and  
 9 the results of the amplitude of the first mode  $a$  can be obtained, which presents the location of the lateral  
 10 connection axially and circumferentially. In this paper, the amplitude of the first mode  $a_{10,v}(z_j)$  (see  
 11 Eq. (7)) is plotted in colourmap, where  $z_j$  is the axial coordinates,  $v$  is the index number of the estimated  
 12 circumferential position of the artefacts (see Figure 4).

13 The number of the microphones in the array used in our measurement determination was  $Q = 6$  (see  
 14 section IV). In this simulation the number of microphones in the array was varied from 5 to 24.



15



1

2

3

4

5

6

7

8

9

10

11

12

Figure 7. a) an illustration of a pipe with a lateral connection; estimation results of b) 24, c) 6 and d) 5 microphones for the location of left lateral connection. The colourmaps are plotted for the amplitude of the first mode  $a_{10,v}(z_j)$ . Yellow colour background denotes the zero amplitude of the first mode  $a_{10,v}(z_j)$  which means empty main pipe, and red colour denotes the angular and axial position of the pipe features.

Figure 7(a) illustrates schematically the setup used in the numerical simulation. The results shown in Figure 7 (b) suggest that the location of the lateral connection is determined at a higher resolution when using 24 microphones (see Figure 7(b)) than when using 6 microphones (see Figure 7(c)). The prediction errors of the axial location of lateral connection are 1.5% for 24, 6, and 5 microphones. The circumferential prediction errors are around  $0^\circ$ ,  $3^\circ$ ,  $9^\circ$  for 24, 6, and 5 microphones, respectively.

The axial location  $\varepsilon$  and circumferential location  $\varepsilon_\theta$  prediction error of the pipe feature is estimated using:

$$\varepsilon = \frac{|z_p - z_r|}{z_r}, \varepsilon_\theta = |\theta_p - \theta_r| \quad (17)$$

13

14

15

16

17

where  $z_p$  and  $z_r$  are the predicted and real locations of the pipe feature, respectively;  $\theta_p$  and  $\theta_r$  are the predicted and real circumferential locations of the pipe feature, respectively. In Figure 7(d), using 5 microphones in a ring (with the absence of a microphone at  $315^\circ$  from 6 microphone array), the location of the lateral connection can still be estimated accurately with less than 2% of the sensing distance in axial prediction error and less than  $9^\circ$  circumferential prediction error.

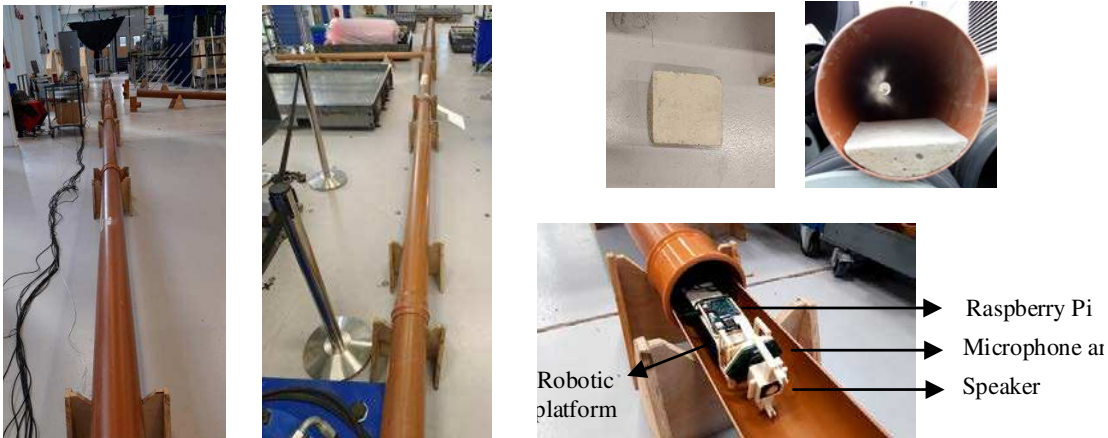
#### 18 IV. Measurement setup

19

20

An measurement was carried out in the iCAIR laboratory at Sheffield ([www.icaire.ac.uk](http://www.icaire.ac.uk)) to validate the method proposed in Section III. A 16 m long uPVC drainage pipe with the 150 mm diameter of the

1 straight pipe section was used in this measurement (see Figure 8 (a)). The straight section was  
 2 terminated with a heavy wooden board at each end, which can be assumed as a rigid reflector, i.e. no  
 3 more than 1% of sound energy was absorbed by this termination in the adopted frequency range. The  
 4 straight section had a 100 mm diameter lateral connection attached at 90° (see Figure 8(b)). A concrete  
 5 insert was used to simulate a 20% blockage at the bottom of the pipe as shown in Figure 8(c).  
 6 The acoustic sensing system was mounted on a remotely controlled robot (iRobot Looj 330 by iRobot,  
 7 www.irobot.com). Acoustic sensors used in this work consisted of a loudspeaker, six-microphone array  
 8 and processor (including power amplifier for loudspeaker, ADC, DAC and Raspberry Pi 4 for data  
 9 acquisition as shown in Figure 8(d) with the sampling rate at 16 kHz and 32 bit resolution. A 100 –  
 10 5000 Hz sweep sine with duration 10 s was used as the excitation signal. The speaker and microphone  
 11 array were located at the centre of the pipe within 5 mm positional mean error initially, although this  
 12 could change due to the robot movement inside the pipe. The microphone type used in this measurement  
 13 was MSM321A3729H9CP by MEMSensing Microsystems Co. Ltd. A Visaton 2242 speaker with the  
 14 32mm diameter was driven with a 3W power supply.



16 *Figure 8. (a) the 150 mm diameter uPVC straight pipe in the iCAIR laboratory, (b) the 150 mm pipe with a 3 m 100 mm lateral*  
 17 *connection, (c) a 20% blockage, (d) the robotic platform with acoustic sensors*

18 **V. Results**

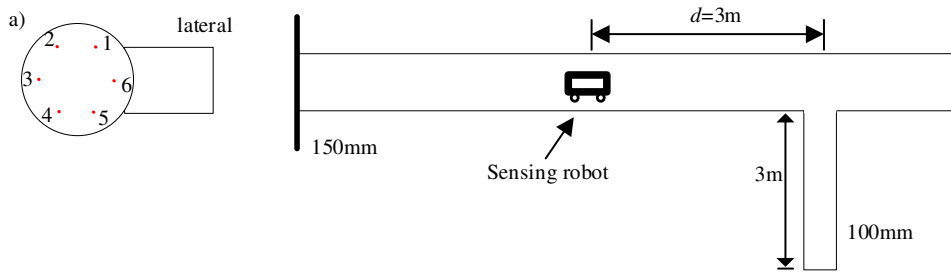
19 The speaker was located at the centre of the 150 mm pipe to excite the plane wave only in the frequency  
 20 range below 2000 Hz (see Figure 2(a)). In this frequency range when the excited plane wave hits the

1 lateral connection or blockage, the reflected wave contains both the plane wave mode and the first non-  
 2 axisymmetric mode. The other modes can also be excited, but they are evanescent and attenuate very  
 3 quickly. Different from the previous study based on the analysis of the plane wave only [5], this paper  
 4 makes use of the behaviour of the first mode to estimate the circumferential orientation of the artefact.  
 5 The time impulse response from each microphone can be obtained by using the deconvolution:

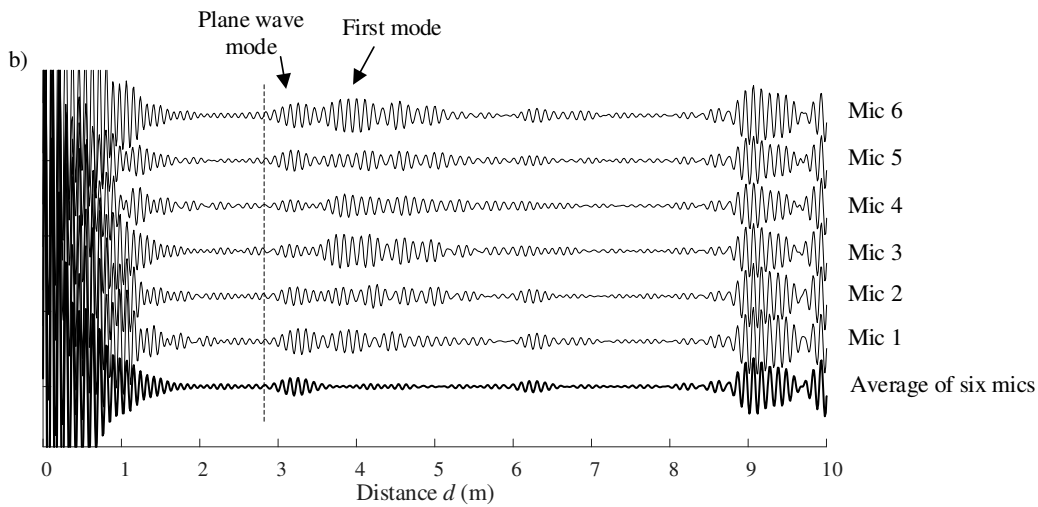
$$\tilde{p}_m(t) = \mathcal{F}^{-1} \left\{ \frac{\mathcal{F}[p_m(t)]}{\mathcal{F}[e(t)] + \alpha} \right\} \quad (18)$$

6 where  $\alpha$  is the regularization factor, which is equal to 0.01 in this experiment,  $e(t)$  is the excitation  
 7 signal as a function of the time  $t$  and  $p_m$  is the sound pressure recorded by the microphone  $m$ .  $\mathcal{F}$  and  
 8  $\mathcal{F}^{-1}$  denote the Fourier and inverse Fourier transforms, respectively. In the following sections the time  
 9 domain impulse response is presented as a function of the distance  $d$  by multiplying the time by sound  
 10 velocity ( $c_0=343$  m/s) and dividing it by 2, i.e.  $d = c_0 t/2$ .

### 11 A. Lateral Connection



12



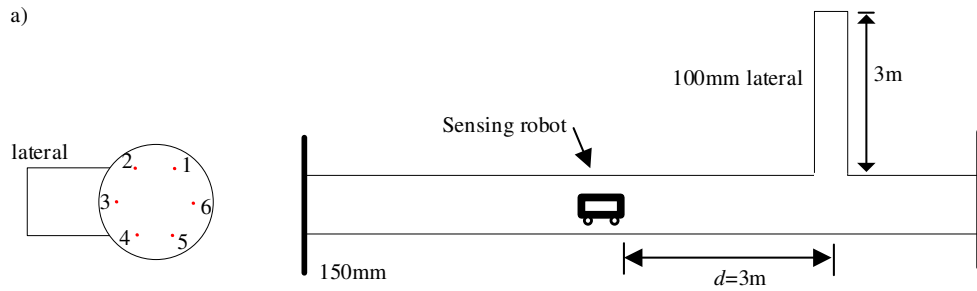
13

1 *Figure 9. (a) An illustration of the setup to localize a lateral connection on the right of the pipe. (b) The corresponding impulse*  
2 *response recorded with the six microphones and filtered in the frequency range of 1500-2000 Hz. The time domain impulse*  
3 *response is presented here and elsewhere as a function of the distance by multiplying the time by the sound velocity (343 m/s)*  
4 *and dividing it by 2.*

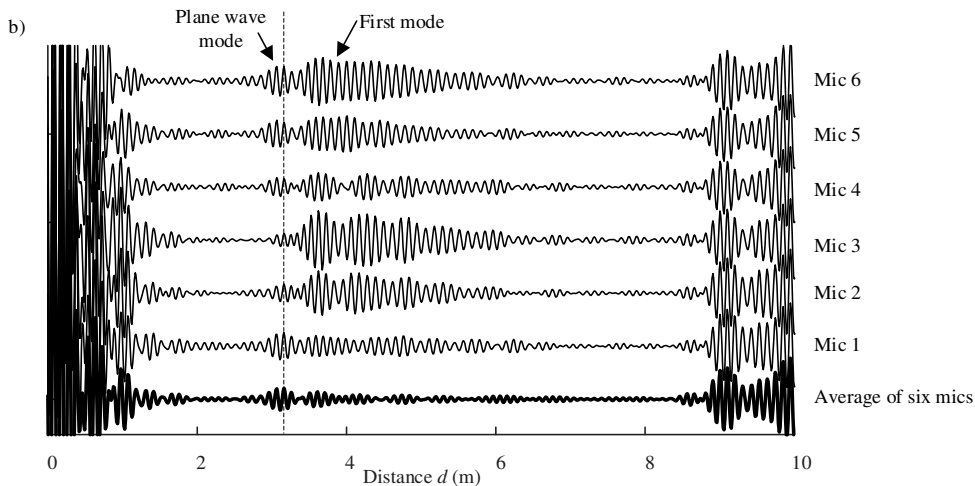
5 Figure 9(a) illustrates the measurement setup with a 100 mm diameter lateral connection on the right-  
6 hand side of the pipe. It also presents the acoustic impulse responses of the six microphones calculated  
7 with Eq. (18) and filtered in the frequency range of 1500 – 2000 Hz, i.e. above the first cut-off frequency  
8  $f_{10}$ . The data were filtered using 6<sup>th</sup> order Butterworth bandpass filter. Figure 9(b) shows the plane wave  
9 and first mode reflected from the lateral connection. The first mode has a lower group velocity than that  
10 of the plane wave. Therefore, this wave arrives to the microphone array at a phase delay.

11 Note that both microphones and loudspeakers are collocated on the robot. In this case, the sound  
12 scattered from the robot itself would affect the signal emitted by the speaker and recorded in the  
13 measurement. This effect is unavoidable and difficult to compensate for accurately without going in  
14 great computational expense to predict the influence of the robot's body through a full numerical  
15 simulation. This effect may cause a blind detection zone for the artefacts/defects' detection. This effect  
16 deserves a separate investigation. However, there is no evidence that the presence of the robot's body  
17 had a significant on the quality of the analysis method presented in this paper as the results presented  
18 in this section illustrate.

19 Similarly, Figure 10(a) illustrates the measurement setup with a lateral connection on the left of the  
20 pipe. Figure 10(b) presents the impulse response from the six microphones filtered in the frequency  
21 range of 1500 – 2000 Hz. Again, the first mode has a lower group velocity than that of the plane wave.  
22 The phase delay can be accounted using the phase compensation term  $e^{i[\gamma_{10}(f_l) + \gamma_{00}(f_l)]z_j}$  in the transfer  
23 matrix  $\mathbf{h}_{10,qv}$  in Eq. (7).



1



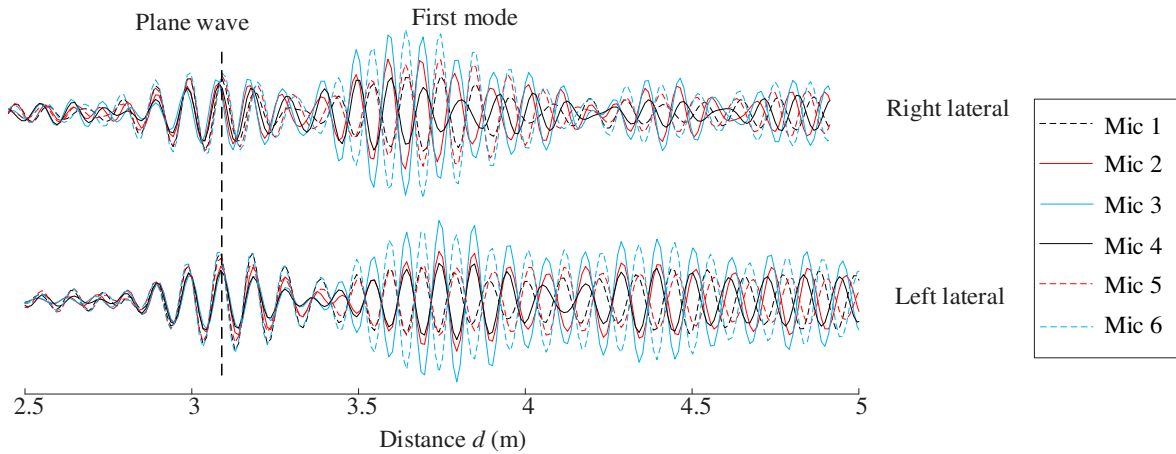
2

3 *Figure 10. (a) An illustration of the setup to localize a lateral connection on the left of the pipe. (b) The corresponding impulse*  
 4 *response recorded with the six microphones and filtered in the frequency range of 1500-2000 Hz.*

5 Figure 11 provides a detailed illustration of the behaviour of the phase in the filtered impulse response  
 6 captured with six microphones in the array. This figure specifically zooms in on the part of the impulse  
 7 response that corresponds to the waves reflected from the lateral connection attached to the right (top  
 8 plot) and left (bottom plot) of the pipe. The data suggest that the phase of the plane wave does not  
 9 change significantly with the microphone position whereas the wave corresponding to the first mode  
 10 does. The plane wave can only be used to estimate the axial location of the lateral connection because  
 11 it does not contain any information about the circumferential position of the artefact. However, the first  
 12 mode can be used to estimate the axial location and circumferential position of this connection. The  
 13 reflected waves propagated as the first mode are out of phase when recorded on a microphone on the  
 14 left in the pipe (e.g. microphone 2, 3 or 4 in Figure 9(a)) and microphone on the right (e.g. microphone  
 15 1, 6 or 5 in Figure 9(a)). In particular, the graphs presented in Figure 11 suggest that the amplitudes and  
 16 phases of microphone pairs 2 and 4 and 1 and 5 are closely aligned. This observation supports the

1 simulation results of the reflected wave patterns presented in Figure 5 revealing that the first mode is  
 2 non-axisymmetric with respect to the vertical diameter of the pipe cross-section (see patterns 2 or 4 in  
 3 Figure 5). This mode carries phase information about the circumferential position of the lateral  
 4 connection. The waves propagated as the first mode swap the phase when the position of the lateral  
 5 connection is changed from left to right (compare the results shown in the top and bottom graphs in  
 6 Figure 11). This is a characteristic that can be intuitively understood from the anti-symmetry of the first  
 7 mode reflected from a lateral connection as illustrated in section III with the FEA simulation (see Figure  
 8 5). Consequently, this phase information associated with the first mode can be used to estimate the  
 9 circumferential position of the lateral connection using a robot equipped with a cross-sectional  
 10 microphone array or a pair of microphones spaced accordingly.

11 Note that mismatches in the amplitude and phase of the plane wave or the first non-axisymmetric mode  
 12 can exist due to the imperfect alignment of the sensor array on the mobile robot. These can also be  
 13 caused by scattering of sound by the robot's body. In our measurement the algorithm was found to work  
 14 when the maximum amplitude difference was 53% and the maximum phase mismatch was 0.3 rad.



15  
 16 *Figure 11. A zoom-in view of the filtered impulse response of the lateral connection on the right (top plot) and on the left*  
 17 *(bottom plot).*

## 18 **B. Blockage**

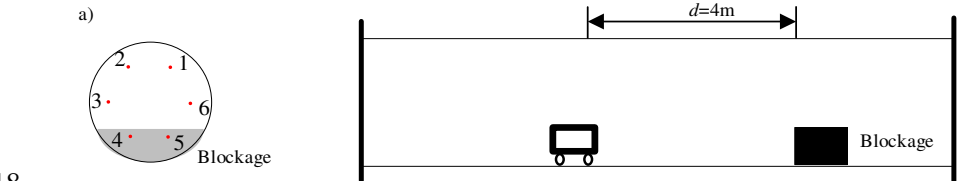
19 The phase difference phenomenon described in the previous section can also be observed in the case of  
 20 a blockage located at the bottom of the pipe. It was demonstrated in an measurement set-up illustrated  
 21 in Figure 12. The blockage ratio ( $h/2R$ , where  $h$  is the blockage depth,  $R$  is the radius of the pipe) is 20%

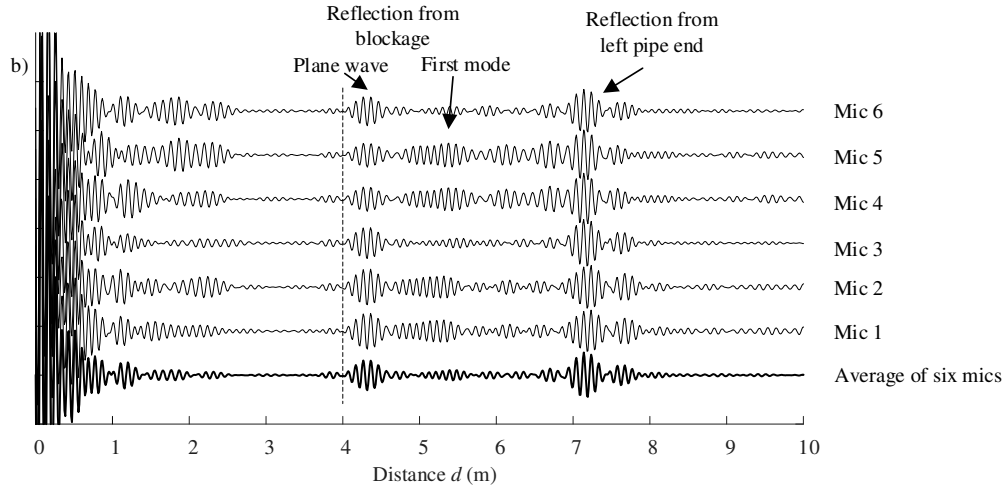
1 and the length of the blockage is 150 mm, as shown in Figure 8(b). The amplitude of the first mode of  
2 sound reflection from a blockage, as measured by microphone 3 and 6, is significantly lower than that  
3 measured by the other microphones. This observation indicates that the modal node is horizontal, and  
4 the peak amplitude is situated at either the top or the bottom of the pipe cross-section.

5 Note that the acoustic wave received within the first 15 ms (corresponds to 2.5 m in the pipe in Figure  
6 12 (b)) are from the initial pulse from the speaker. This near-field sensing due to the closely positioned  
7 speaker and microphone can result in cross-talking between the microphone, speaker and the robot body.  
8 Some higher evanescent wave modes may also be sensed by the microphone from the speaker.  
9 Therefore, the first 12 ms (corresponds to 2 m in the pipe) is regarded as a “blind zone” in this proposed  
10 method. The pipe end is located around 7 m away from the blockage which does not impact on the  
11 results.

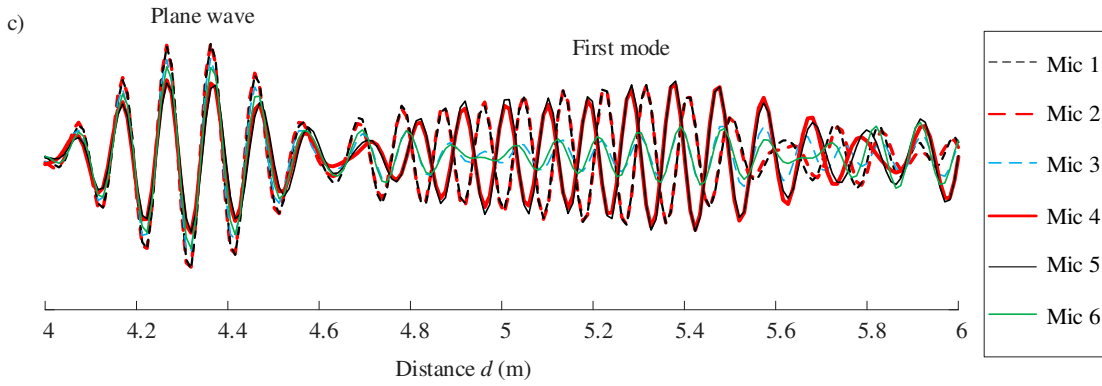
12 To emphasize the microphone array characterization of the blockage, a zoom-view of the acoustic wave  
13 from each microphone between 4-6 m is shown in Figure 12 (c). As a result, microphone pairs 1-2 and  
14 4-5 are expected to exhibit identical amplitude, a fact that is confirmed in Figure 12 (c). In addition,  
15 microphones 1 and 5 display opposite phase response for the first mode, as demonstrated in Figure 12  
16 (c).

17





1



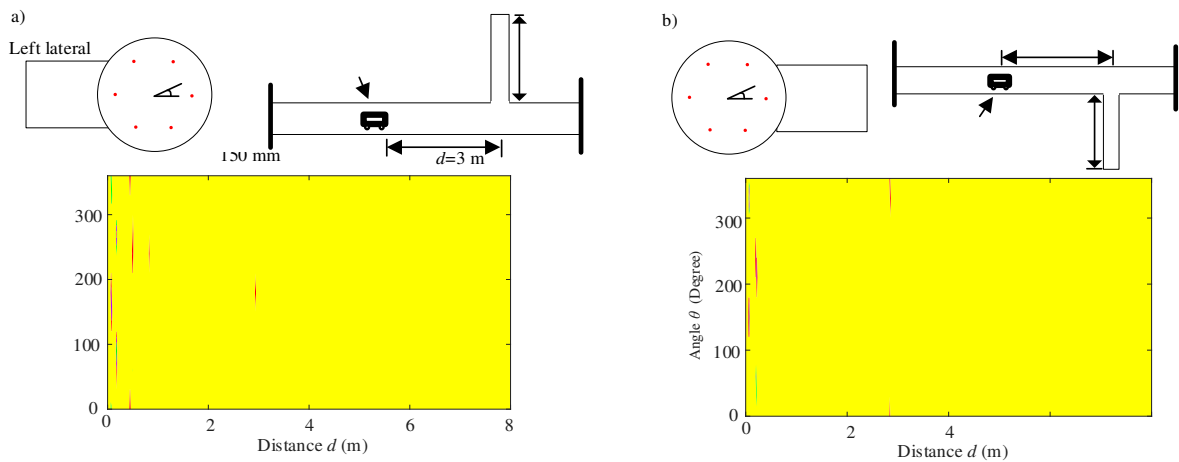
2

3 *Figure 12. (a) An illustration of using six microphones for the localization of a blockage, (b) impulse response of six*  
 4 *microphones estimated using Eq. (18) over the frequency range 1500-2000 Hz c) a zoom-in view of the impulse response from*  
 5 *the blockage reflection. The curves measured by microphones 1 and 2 exhibit convergence, as do those of microphones 3 and*  
 6 *6, and microphones 4 and 5 similarly manifest a state of convergence.*

### 7 **C. Lateral connection and blockage localization**

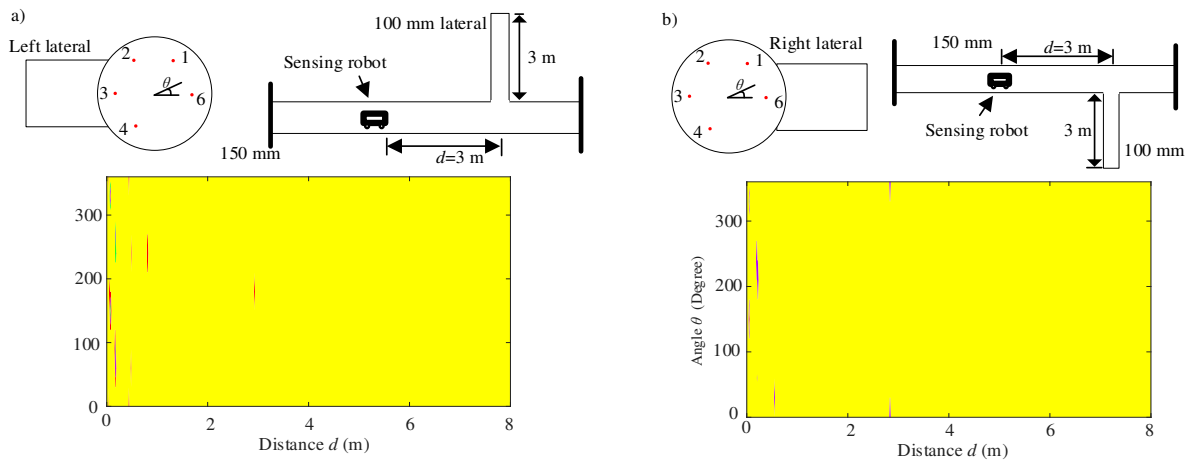
8 In Figure 13, the outcomes of localizing lateral connections are presented, where the amplitude of the  
 9 first mode  $a_{10,v}(z_j)$  (see Eq. (7)) is plotted in colourmap. The localization process utilizes information  
 10 obtained from the first mode measurement with six microphones in an measurement with the lateral  
 11 connection being on the left and on the right of the main pipe. Consistent with simulation findings, the  
 12 estimated axial location of the lateral connections was found to be 2.94 m and 2.93 m, respectively,  
 13 with less than 2% of the sensing distance estimation error. The sensing blind zone, associated with the  
 14 initial pulse and the near-field effects, was determined to be within 2m. The proposed algorithm that  
 15 combines the phase information of the lateral reflection pulse accurately estimated the circumferential  
 16 location of the lateral direction. As shown in Figure 13, the predicted mean angular position of the

1 lateral is at  $182^\circ$  for left lateral ( $2^\circ$  prediction error), while the predicted angular position of the right  
 2 lateral is around  $3$  or  $363^\circ$  ( $<3^\circ$  prediction error).



3  
 4 *Figure 13. An measurement localization of a lateral connection using a six-microphone array: (a) connection on the left; (b)*  
 5 *connection on the right. Yellow colour background denotes the zero amplitude of the first mode  $a_{10,v}(z_j)$  which means empty*  
 6 *main pipe, and red colour denotes the angular and axial position of the pipe features.*

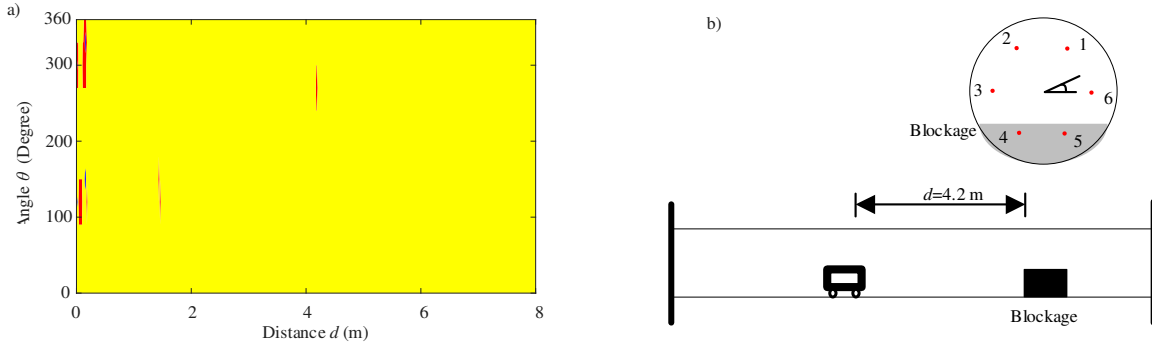
7 Figure 14 illustrates the estimation outcome utilizing a 5-microphone array, wherein the 5<sup>th</sup> microphone  
 8 is not present. Consistent with simulation findings, the estimated axial location of the lateral connection  
 9 was found to be 2.94 m, and 2.93 m, respectively, with less than 2% of the sensing distance error.



10  
 11 *Figure 14. An measurement localization of a lateral connection using a five-microphone array: (a) connection on the left; (b)*  
 12 *connection on the right. Yellow colour background denotes the zero amplitude of the first mode  $a_{10,v}(z_j)$  which means empty*  
 13 *main pipe, and red colour denotes the angular and axial position of the pipe features.*

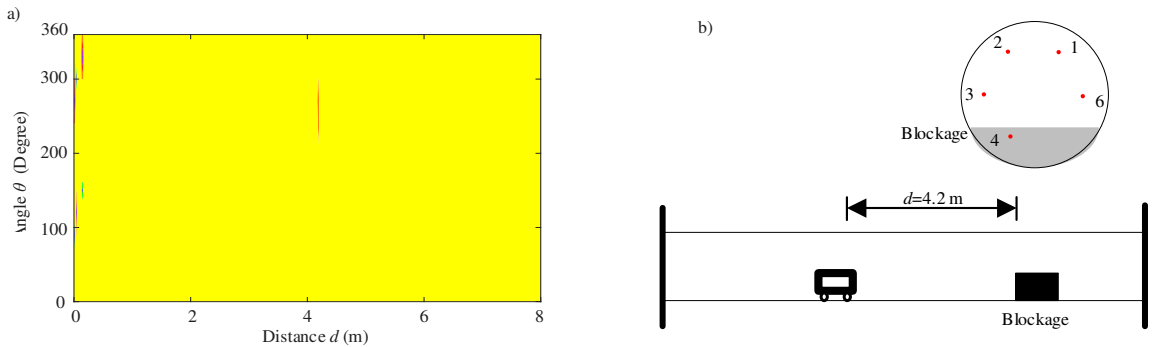
14  
 15 The Bayesian estimation results for blockage localization in the pipe are presented in Figure 15. The  
 16 estimated axial location of the blockage with 6 microphones is 4.18 m and estimation error are less than

1 0.5% of the sensing distance error. The central position of the blockage is predicted at the bottom of the  
 2 pipe at  $265^\circ$  (with  $5^\circ$  prediction error), as illustrated in Figure 15a. Notably, a significant noise at  
 3 approximately 1.5 m which is due to detection blind zone of this method caused by the phenomena as  
 4 discussed in Section V.B.



5  
 6 *Figure 15. the blockage localization result using 6 microphones. Yellow colour background denotes the zero amplitude of the*  
 7 *first mode  $a_{10,v}(z_j)$  which means empty main pipe, and red colour denotes the angular and axial position of the pipe features.*

8 The Bayesian estimation results for blockage localization in the pipe are presented in Figure 16. Similar  
 9 to the case with 6 microphones, the estimated axial location of the blockage using a 5-microphone array  
 10 is 4.18 m, with an estimation error of less than 0.5% of the sensing distance. The central position of the  
 11 blockage is predicted to be located at the bottom of the pipe at  $263^\circ$  (with  $7^\circ$  prediction error), as  
 12 illustrated in Figure 16(a).



13  
 14 *Figure 16. The blockage localization result using 5 microphones. Yellow colour background denotes the zero amplitude of the*  
 15 *first mode  $a_{10,v}(z_j)$  which means empty main pipe, and red colour denotes the angular and axial position of the pipe features.*

16

## 17 D. Conclusions

18 Determining both axial location and circumferential position of an artefact is important when using

1 inspection information for determining the need to map, repair or to clean drainage pipes. Traditional  
2 sewer defect classification schemes (WRc, 2013 [19]) that currently require the analysis of CCTV  
3 images need such positional information when fully classifying artefacts/defects. Circumferential  
4 position is important as this determines at which water level that a defect or connection starts to have a  
5 significant impact on the hydraulic carrying capacity of the pipe.

6 This paper proposed a Bayesian learning method and use of the first propagation wave mode to detect  
7 and localize pipe features axially and circumferentially. This method is validated against numerical and  
8 measurement data with a 150 mm diameter pipe with a 100 mm diameter lateral connection and 20%  
9 in-pipe blockage. The accuracy of localization of the lateral connection and blockage attained in this  
10 measurement was better than 2% of the sensing distance for the axial location prediction, and 9° error  
11 for the circumferential location prediction. This work paves the way for the development of new  
12 acoustic instrumentation for the rapid condition assessment in dry and partially filled pipes, e.g. sewer  
13 and drainage pipes.

14 The presence of a water layer in the pipe changes the mode shapes [8]. For example, in a partially filled  
15 pipe the non-axisymmetric mode can split into two different modes whereas the axisymmetric mode  
16 does not. New experimental data and simulations are required to understand the scattering modal  
17 patterns from an artefact in a partially filled pipe to apply the proposed method with compensation for  
18 the water level effect. To the best of our knowledge this has not been done before so that it should be  
19 the focus of our future work.

#### 20 **E. Conflict of Interest statement and Data Availability**

21 All authors (Yicheng Yu, Kirill V. Horoshenkov, and Simon Tait) declare that they have no conflict of  
22 interest or financial conflicts to disclose. The data that support the findings of this study are available  
23 from the corresponding author upon reasonable request.

24

#### 25 **F. Acknowledgement**

26 This work is supported by the UK's Engineering and Physical Sciences Research Council (EPSRC)

1 Programme Grant EP/S016813/1. The authors would like to gratefully thank Mr. Gavin Sailor for kindly  
2 helping the design of the robotic platform to support the acoustic sensing system. The authors would  
3 also like to gratefully thank Dr. Will Shepherd and Mr. Paul Osbourne for kindly helping the design of  
4 the blockages and providing other measurement facilities. For the purpose of open access, the authors  
5 have applied a ‘Creative Commons Attribution (CC BY) licence to any Author Accepted Manuscript  
6 version arising’.

## 7 **G. References**

8

- [1] “Discover water: treating sewage,” [Online]. Available: <https://discoverwater.co.uk/treating-sewage>. [Accessed 01 02 2023].
- [2] T. L. Nguyen, A. Blight, A. Pickering, G. Jackson-Mills, A. R. Barber, J. H. Boyle, R. Richardson, M. Dogar and N. Cohen, “Autonomous control for miniaturized mobile robots in unknown pipe networks,” *Frontiers in Robotics and AI*, vol. 9, no. 16, 2022.
- [3] Y. Yu, A. Safari, X. Niu, B. Drinkwater and K. V. Horoshenkov, “Acoustic and ultrasonic techniques for defect detection and condition monitoring in water and sewerage pipes: A review,” *Applied Acoustics*, vol. 183, no. 0003-682X, p. 108282, 2021.
- [4] J. M. Aitken, M. H. Evans, R. Worley, S. Edwards, R. Zhang, T. Dodd, L. Mihaylova and S. R. Anderson, “Simultaneous localization and mapping for inspection robots in water and sewer pipe networks: A review,” *IEEE Access*, vol. 9, 2021.
- [5] Y. Yu, R. Worley, S. Anderson and K. V. Horoshenkov, “Microphone array analysis for simultaneous condition detection, localization, and classification in a pipe,” *The Journal of the Acoustical Society of America*, vol. 153, no. 367, p. 367–383, 2023.
- [6] P. M. Morse and K. U. Ingard, *Theoretical acoustics*, Princeton university press, 1986.

- [7] Y. Yu, A. Krynkina, Z. Li and K. V. Horoshenkov, “Analytical and empirical models for the acoustic dispersion relations in partially filled water pipes,” *Applied Acoustics*, vol. 179, no. 0003-682X, p. 108076, 2021.
- [8] R. Worley, Y. Yu and S. Anderson, “Acoustic Echo-Localization for Pipe Inspection Robots,” in *2020 IEEE International Conference on Multisensor Fusion and Integration for Intelligent Systems (MFI)*, 2020.
- [9] C. C. Paige and M. A. Saunders, “LSQR: An algorithm for sparse linear equations and sparse least squares,” *ACM Transactions on Mathematical Software (TOMS)*, vol. 8, no. 1, pp. 43-71, 1982.
- [10] S. L. Brunton and J. N. Kutz., *Data-driven science and engineering: Machine learning, dynamical systems, and control.*, Cambridge University Press, , 2019..
- [11] S. V. Vaseghi, *Advanced digital signal processing and noise reduction*, John Wiley & Sons, 2008.
- [12] N. Xiang, “Model-based Bayesian analysis in acoustics—A tutorial,” *The Journal of the Acoustical Society of America* 148.2, pp. 1101-1120, 2020.
- [13] N. Xiang and C. Fackler, “Objective Bayesian analysis in acoustics,” *Acoustics Today*, vol. 11, no. 2, pp. 54-61, 2015.
- [14] M. Belge, M. E. Kilmer and E. L. Miller, “Wavelet domain image restoration with adaptive edge-preserving regularization,” *IEEE Transactions on Image Processing* , vol. 9, no. 4, pp. 597-608, 2000.
- [15] M. A. Figueiredo, “Adaptive sparseness for supervised learning,” *IEEE transactions on pattern analysis and machine intelligence*, vol. 25, no. 9, pp. 1150-1159, 2003.
- [16] S. D. Babacan, R. Molina and A. K. Katsaggelos, “Bayesian compressive sensing using Laplace priors,” *IEEE Transactions on image processing*, vol. 19, no. 1, pp. 53-63, 2009.

- [17] S. J. Wright, R. D. Nowak and M. A. Figueiredo, "Sparse reconstruction by separable approximation," *IEEE Transactions on Signal Processing*, vol. 57(7), pp. 2479-2493, 2009.
- [18] J.-P. Berenger, "A perfectly matched layer for the absorption of electromagnetic waves," *Journal of computational physics*, vol. 114, no. 2, pp. 185-200, 1994.
- [19] WRc, "Manual of Sewer Condition Classification," MSCC, 5th Edition, 2013. [Online]. Available: <https://wrcknowledgestore.co.uk>. [Accessed 27 9 2023].

1

2